ACS APPLIED MATERIALS & INTERFACES

Research Article

www.acsami.org

Simple Microfluidic Approach to Fabricate Monodisperse Hollow Microparticles for Multidrug Delivery

Remigijus Vasiliauskas,[†,‡] Dongfei Liu,[‡] Salvatore Cito,[‡] Hongbo Zhang,[‡] Mohammad-Ali Shahbazi,[‡] Tiina Sikanen,[‡] Linas Mazutis,*[,†,§] and Hélder A. Santos*[,‡]

[†]Vilnius University Institute of Biotechnology, Vilnius LT-02241, Lithuania

[‡]Division of Pharmaceutical Chemistry and Technology, Faculty of Pharmacy, University of Helsinki, Helsinki FI-00014, Finland

[§]School of Engineering and Applied Physics, Harvard University, Cambridge, Massachusetts 02138, United States

ABSTRACT: Herein, we report the production of monodisperse hollow microparticles from three different polymers, namely, pH-responsive acetylated dextran and hypromellose acetate succinate and biodegradable poly(lactic-*co*-glycolic acid), at varying polymer concentrations using a poly(dimethylsiloxane)-based microfluidic device. Hollow microparticles formed during solvent diffusion into the continuous phase when the polymer close to the interface solidified, forming the shell. In the inner part of the particle, phase separation induced solvent droplet formation, which dissolved the shell, forming a hole and a hollow-core particle. Computational simulations showed that, despite the presence of convective recirculation around the droplet, the mass-transfer rate of the solvent dissolution from the droplet to the surrounding phase was dominated by diffusion. To illustrate the potential use of hollow microparticles, we simultaneously encapsulated two anticancer drugs and investigated their loading and release profiles. In addition, by utilizing different polymer shells and polymer concentrations, the release profiles of the model drugs could be tailored according to specific demands and applications. The high encapsulation efficiency, controlled drug release, unique hollow microparticle structure, small particle size (<7 μm), and flexibility of the polymer choice could make these microparticles advanced platforms for pulmonary drug delivery.

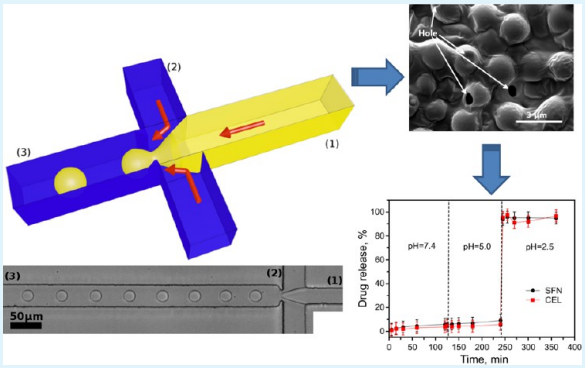

KEYWORDS: *hollow microparticles, PDMS microfluidics, solvent diffusion, drug delivery, multidrug encapsulation*

1. INTRODUCTION

As a result of great advances in materials science, physics, biology, and nanotechnology, diverse types of drug-delivery systems are available today.[1−3] Drug-loaded micro- and nanoparticles are among the most promising systems for targeted and controlled drug delivery and noninvasive drug administration. The vast majority of the techniques being used for the preparation of drug-loaded microparticles are based on conventional technologies, for example, homogenization,[4] mechanical stirring, and sonication.[5] However, these conventional methods do not provide control of the physicochemical properties of the generated microparticles. In particular, the high polydispersities of the obtained particles [coefficient of variation (CV) of ∼10−30%][6−8] impose several limitations on the wide application of these conventional methods. The broad size distributions of the particles lead to poor control over the kinetics of drug release and contribute to uncontrolled variations in the rate of particle degradation. In contrast, monodisperse drug-loaded particles offer significantly better control over the drug release kinetics and minimize the undesired "burst-release" phenomenon that is commonly observed with polydisperse particles.[6] The droplet-based microfluidic approach enables the production of monodisperse microparticles with precisely controlled particle sizes and, thus, circumvents current limitations on particulate drug-delivery systems.[9]

Because of its large epithelial surface area (80−140 m^2), high organ vascularization, extremely thin (0.1−2-μm) blood−air barrier, and immense capacity for solute exchange, lung tissue is an ideal noninvasive administration route for the absorption of significant amounts of drugs.[10] Pulmonary drug delivery is a highly desirable option as it allows local and systematic targeting, lower administered dosages, and reduced side effects of drugs.[11] However, conventional carriers usually exhibit uncontrolled drug delivery and premature drug release, which can result in a sharp increase in drug concentrations to potentially toxic levels. To prevent such undesirable toxicity, the release of the cargo should be performed in a controllable manner. For this reason, several groups have used biodegradable and environmentally sensitive polymers for the production

Received: April 15, 2015
Accepted: June 22, 2015
Published: June 22, 2015

DOI: 10.1021/acsami.5b04824
ACS Appl. Mater. Interfaces 2015, 7, 14822−14832

of drug-loaded particles.[12−15] Unfortunately, despite their biocompatible properties, the large sizes of such particles (30−130 μm) impose limitations for pulmonary drug-delivery applications. In particular, porous or hollow particles are preferred because they are more easily transported by air and, on account of their lower densities, can penetrate lung capillaries more efficiently than solid particles.[11,16] The most common methods for producing porous or hollow particles are layer-by-layer fabrication[17] and stirring followed by solvent evaporation.[18] These methods, however, consist of several preparation steps and suffer from poor uniformity of the resulting particles.

Significant advances have been made in the preparation of micro- and nanoparticles with microcapillary devices.[13,14,19−24] These devices can generate hollow particles by encapsulating gas as the inner phase[25] and can be used to prepare monodisperse porous and hollow particles using the solvent evaporation method.[26] However, microcapillary devices allow the production of only relatively large (typically 50−300-μm) microparticles.[27] For pulmonary applications, aerodynamic particles in the size range of 1−5 μm are desirable, although they can have an actual size of 1−20 μm depending on the particle shape, weight, and porosity.[11,28−30] Poly(dimethylsiloxane)- (PDMS-) based microfluidic devices fill this gap and allow the production of particles from 0.1 to 100 μm in size,[31,32] making it a suitable platform for producing particles intended for pulmonary drug delivery. PDMS-based microfluidic devices have been continuously used for the production of hydrogel microparticles, the encapsulation of cells, and the delivery of water-soluble drugs.[33−35] Because of their transparency to light with wavelengths greater than 230 nm, PDMS-based microdevices have been used to produce particles with different sizes and shapes by UV-curing polymers in the microchannels.[31] It has also been demonstrated that PDMS microfluidics can be used to produce microparticles by solvent extraction and evaporation methods.[32]

When droplets are produced inside a microfluidic device, diffusion and convection are the two major mechanisms responsible for the mass-transfer rate. Diffusion is determined by the diffusion coefficient, whereas convection depends on many factors that are device-dependent. Specifically, for microfluidic devices that operate in the two-phase flow regime with a moving meniscus, there are two possible scenarios: (a) the presence of capillary-driven flow in which the meniscus wets the wall and (b) the presence of droplets that are dragged by the main phase flow. In the former case, convection is caused by the inertia of the meniscus, which depends on the slip velocity at the triple point[36,37] and the shape of the microchannel, whereas in the latter case, convection is caused only by the inertia of the meniscus, which depends on the droplet size and the shape of the microchannel.[38]

In this work, we present a simple and robust approach to generate monodisperse hollow microparticles using a PDMS-based microfluidic device. Microparticles were produced using the pH-sensitive polymers acetylated dextran (Ac-Dex) and hypromellose acetate succinate (HPMC-AS) and the biodegradable polymer poly(lactic-*co*-glycolic acid) (PLGA). We found experimentally that the formation of hollow microparticles is independent of the polymer used. We also performed numerical simulations of the experimental setup to better assess the role of diffusion and convection in the mass-transfer rate around the droplet during incubation on-chip. We propose a model according to which solvent diffusion from the droplet induces shell solidification and inner phase separation. Two anticancer model drugs, sorafenib (SFN) and celecoxib (CEL), were encapsulated, and their simultaneous release was monitored over time in buffers with different pH values, showing the potential use of hollow microparticles for pulmonary drug-delivery applications.

2. EXPERIMENTAL SECTION

2.1. Materials. Poly(dimethylsiloxane) (PDMS, Sylgard 184 silicone elastomer kit) together with curing agent were purchased from Dow Corning (Midland, MI). Poly(allylamine hydrochloride) (PAH, ∼58 kDa), poly(sodium 4-styrenesulfonate) (PSS, ∼70 kDa), poly(vinyl alcohol) (PVA, 130 kDa, 87% hydrolyzed, ester number 130−150), Tween 80 (79 kDa), dimethyl carbonate (DMC, ≥99%), ethyl acetate (≥99.8%), poly(lactic-*co*-glycolic acid) (PLGA, 50:50, 30−60 kDa), and celecoxib (CEL, ∼381 Da) were purchased from Sigma-Aldrich (St. Louis, MO). Pluronic F127 (9.8−14.6 kDa) was a gift from BASF (Ludwigshafen am Rhein, Germany). Polymer hypromellose acetate succinate (HPMCAS-HF, ∼286 Da) was a gift from HARKE Pharma (Mülheim an der Ruhr, Germany). Acetalated dextran (Ac-Dex, ∼40 kDa) was synthesized as described elsewhere.[20] Sorafenib (SFN, >99%, ∼464 Da) was purchased from LC Laboratories (Woburn, MA). All water used was Millipore MQ-water with a resistivity of 18.2 MΩ cm.

2.2. Fabrication of the PDMS Microfluidic Device. A schematic illustration and optical micrograph of droplet production in the PDMS-based flow-focusing microfluidic device are shown in panels a and b, respectively, of Figure 1. The PDMS microfluidic device was fabricated using soft lithography, as described in detail elsewhere.[39] Briefly, photolithography was used to create a high-aspect-ratio relief feature of the appropriate design in photoresist (SU-8) on a silicon wafer. The feature was then replicated in PDMS by curing the prepolymer against this master. The PDMS replica was subsequently placed on a glass substrate, creating sealed channels. Inlets and outlets were fabricated by punching holes in the PDMS. To produce hydrophilic surfaces in the microfluidic device, the channels were treated using a layer-by-layer method with PAH and PSS.[40] First, the

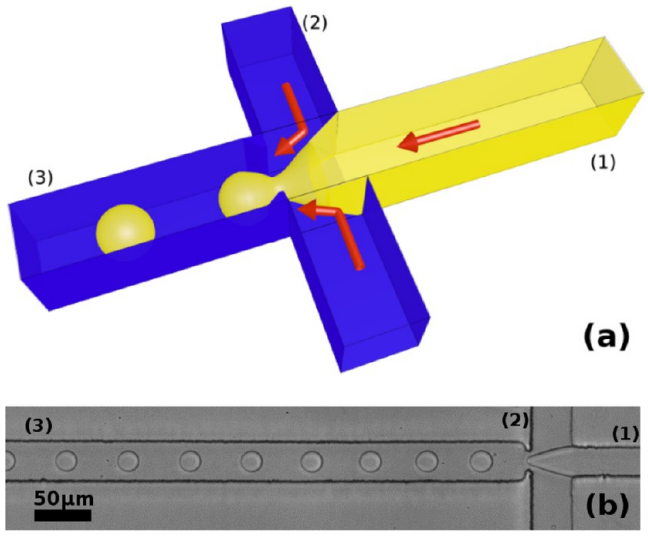

Figure 1. (a) Schematic and (b) optical microscope image of the structure of the microfluidic device used for the production of oil-in-water emulsions. The device consists of two inlets for the (1) dispersed phase (solvent) and (2) continuous phase (water) and a (3) droplet collection outlet. Droplet generation takes place at the junction where the channels for the dispersed and continuous phases meet. Droplets then move downstream along the flow to the collection outlet.

DOI: 10.1021/acsami.5b04824
ACS Appl. Mater. Interfaces 2015, 7, 14822−14832

PDMS device was treated with oxygen plasma for 5 min and bound to the glass slide. Immediately thereafter, the channels of the microfluidic device were filled with PAH (0.5%, w/w) in 0.5 M NaCl solution for 5 min. Next, the channels were washed with 0.1 M NaCl solution. The second layer was generated by filling the channels with PSS (0.5%, w/w) in 0.5 M NaCl. Following a 5-min treatment with PSS, the channels were washed with deionized water. The procedure was repeated twice to improve the hydrophilic layer in the channels.

2.3. Preparation of the Microparticles. For the production of monodisperse oil-in-water droplets and microparticles, a flow-focusing PDMS microfluidic device with 20-μm-deep and 30-μm-wide channels (Figure 1b) and flow rates of 20 and 80 μL/h for the oil and water phases, respectively, were used. The oil and water phases merged into one channel, where droplets were generated. The droplets then traveled to the outlet, were collected through polytetrafluoroethylene (PTFE) tubing in a tube prefilled with a buffer solution, and were left overnight for solvent diffusion to occur. Longer incubations produced a higher uniformity of particles.

As an oil phase, the solvent DMC was chosen. DMC is a green and environmentally benign chemical because of its multiple reactivity and wide potential usage in chemical industry. Additionally, it has low toxicity and fast biodegradation kinetics[41] compared to other commonly used organic solvents for particle production, such as dichloromethane.[42,43] Moreover, it has a moderate solubility in water (up to 13.9%, v/v), low enough for droplet formation and high enough for the solvent to be diffused from the droplets and facilitate the formation of microparticles through polymer precipitation. Most importantly, DMC does not induce PDMS swelling, making it possible to stably generate droplets for long periods of time (>8 h). PVA (2%, w/v) in water was used as the continuous phase.

We used Ac-Dex, HPMCAS-HF, and PLGA polymers, dissolved in DMC, to produce monodisperse droplets in the PDMS microdevice. The polymer solubility in the solvent had no visible effect on the particle morphology. However, an increase in the dispersed-phase viscosity, which varied depending on the type of polymer, had a pronounced effect on the droplet generation process. We found the concentration ranges of 1−10 mg/mL for HPMCAS-HF and 1−100 mg/mL for Ac-Dex to be suitable for the production of highly monodisperse droplets. Ac-Dex was chosen because of its pH-responsiveness, high solubility in DMC, and small increase in viscosity with increasing its concentration. This allowed for the production of Ac-Dex particles over a wider range of concentrations (1−100 mg/mL) than for the other polymers used in this work. Also, Ac-Dex is nontoxic to lung epithelial cells, thus making it a good material for pulmonary drug delivery.[12]

To control the release of the cargo from the formed microparticles under different pH conditions, we used Ac-Dex, which degrades and releases drugs under acidic conditions (pH < 6),[20] and also HPMCAS-HF, which dissolves under basic conditions (pH > 7.4).[14,15] Thus, when these microparticles were produced, the droplets were collected at pH values that ensured the stability of the particles: pH > 7.4 for Ac-Dex and pH < 5 for HPMCAS-HF.

For the production of hollow microparticles with encapsulated drugs, we used 10, 50, and 100 mg/mL Ac-Dex or 10 mg/mL HPMCAS-HF polymer together with 0.5 mg/mL CEL and SFN. The polymer and drugs were dissolved in DMC. After droplet formation, the DMC diffused out of the droplets, but the drug molecules, which are insoluble in water, were trapped in the polymer matrix.

2.4. Numerical Study of the Particle Formation Process. Under no-flow conditions, the mass transfer between a droplet and the surrounding fluid is driven only by diffusion, and the mass-transfer efficiency increases with decreasing droplet size, as the efficiency is proportional to the ratio between the surface area and volume of the droplet. Instead, under flow conditions (as in this study), convection starts to play an important role in mass-transfer efficiency. The inertial forces increase with the size of the droplet (in motion). Consequently, this increases the effect of convection on mass transfer. To examine the competition between diffusion and convection in the mass transfer of the solvent (DMC) from a moving droplet, we developed a computational fluid dynamics (CFD) model that predicts the mass-transfer rates in two-phase flow (solvent droplets in water) in a microchannel.

For the physical model, it is assumed that both phases (water and solvent) are binary mixtures. At $t = 0$, the solvent (DMC) forms a drop with a diameter of D_d, which starts to move driven by the flow of water in a two-dimensional microchannel. Water is pumped from the microchannel inlet at a given volume flow rate of $Q = 20$ μL/h. The width (W) of the channel is 30 μm, and the height (H) is 20 μm. The length scale considered in the numerical solution is $L = 10W$. The diffusion coefficient (k) of the solvent (DMC) is set equal to 3.5×10^{-11} m^2/s. The density and viscosity of water at 25 °C are 1 g/cm^3 and 0.9 mPa s, respectively, and the density and viscosity of oil DMC at 25 °C are 1 g/cm^3 and 0.5 mPa s, respectively.

To describe the physical model mathematically, we used the mass-transfer equation (eq 1), which includes diffusion and convection of dilute species in both phases

$$\frac{\partial c}{\partial t} = \nabla\cdot(k\nabla c)\vec{u}\cdot\nabla c \tag{1}$$

To predict the unknown convective forces described in this equation, eq 1 was coupled with the following momentum equations for incompressible flow

$$\rho\left(\frac{\delta\vec{u}}{\delta t} + \vec{u}\cdot\vec{u}\nabla\right) = -\nabla p + \nabla\cdot\mu[\nabla\vec{u} + (\nabla\vec{u})^{\mathrm{T}}] + \overrightarrow{F_{\mathrm{St}}} \tag{2}$$

$$\nabla\cdot\vec{u} = 0 \tag{3}$$

In these equations, ρ is the density of the fluid, $\vec{u}$ is the velocity vector, p is the pressure, μ is the viscosity, k is the coefficient of diffusivity of the solvent, and c is the concentration of the solvent.

Yue et al.[44] examined the implications of diffusion on mass conservation when using a phase-field model for simulating two-phase flows. They observed that, even though the phase-field variable φ is conserved globally, a drop shrinks spontaneously as φ shifts from its expected value in the bulk phase. These changes were found to be proportional to the interfacial thickness, and they suggested guidelines for minimizing the loss of mass.

In the present study, to capture and track the interface between the two phases, we used the level set method (LSM), which is a phase-field model. In the LSM, a smoothed indicator function φ is transported and reinitialized according to the equation

$$\left(\frac{\delta\varphi}{\delta t} + \vec{u}\cdot\nabla\varphi\right) = \gamma\nabla\cdot\left[\varepsilon\nabla\varphi - \varphi(1-\varphi)\frac{\nabla\varphi}{|\nabla\varphi|}\right] \tag{4}$$

where γ and ε are initialization parameters and φ has values between 0 and 1. At the interface, φ is equal to 0.5.

Finally, for the numerical solution of the system of partial differential equation (eqs 1−4), the commercial finite-element code Comsol Multiphysics 5.0 was used with the following boundary conditions: (a) normal inflow velocity and constant concentration equal to zero at the inlets, (b) constant pressure and zero diffusion flux of the reactant at the outlet, and (c) nonslip conditions at the walls. After mesh- and time-step-independence analyses had been performed, a nonuniform triangular mesh with a maximum size equal to 0.1 μm and a maximum time step equal to 2 μs was used for all simulations. Following the guidelines proposed by Yue et al.,[44] we found that, for a thickness equivalent to 5 μm, mass was still conserved in the numerical solution. Therefore, the transition of the physical properties between the two phases is given by the following equations

$$\rho = \rho_1 + (\rho_2 - \rho_1)\varphi \tag{5}$$

$$\mu = \mu_1 + (\mu_2 - \mu_1)\varphi \tag{6}$$

$$k = k + (k_2 - k_1)\varphi \tag{7}$$

2.5. Characterization of the Microparticles. The morphology, surface topography, and internal structure of the prepared microparticles were evaluated by scanning electron microscopy (SEM). For the studies of internal structure, the microparticles were first

DOI: 10.1021/acsami.5b04824
ACS Appl. Mater. Interfaces 2015, 7, 14822−14832

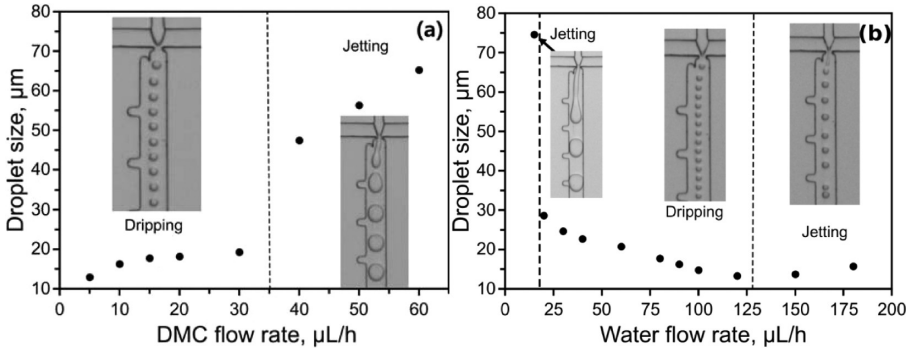

Figure 2. Droplet size as a function of flow rate. The transitions between the dripping and jetting regimes is marked by vertical dashed lines. (a) The flow rate of the continuous phase was set at 80 μL/h, and the flow rate of the dispersed phase was varied from 5 to 50 μL/h. (b) The flow rate of the dispersed phase was set at 15 μL/h, and the flow rate of the continuous phase was varied from 20 to 180 μL/h.

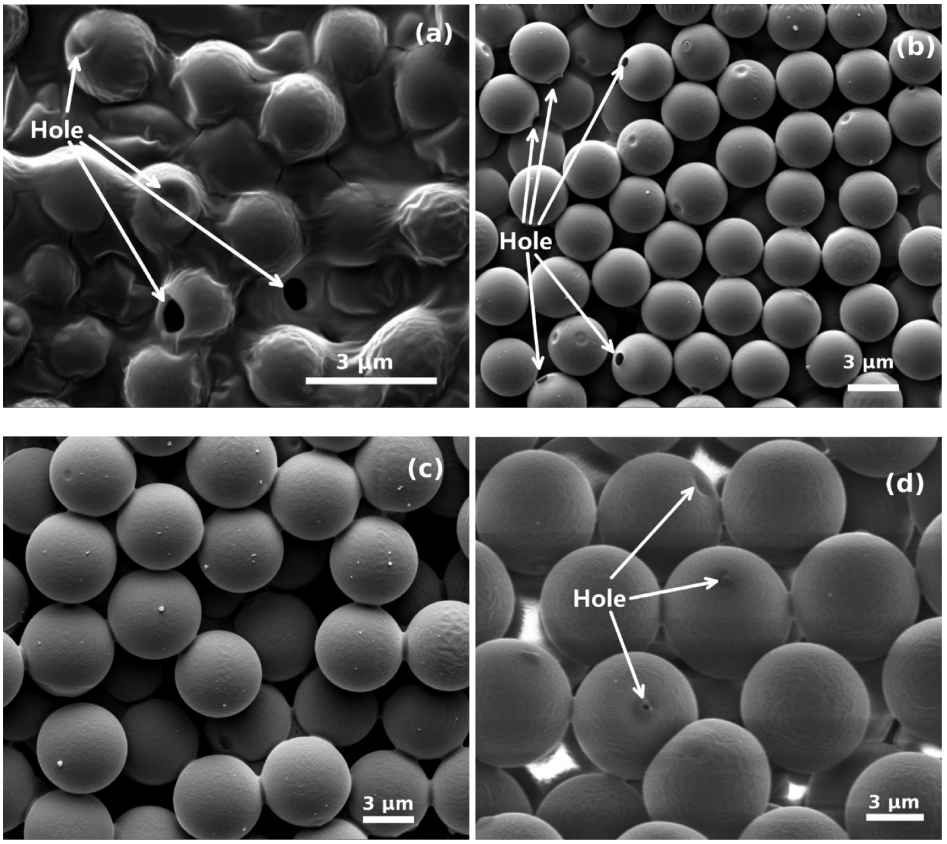

Figure 3. SEM micrographs of Ac-Dex particles prepared with the same microfluidic device and flow rates of 80 and 20 μL/h for the continuous and dispersed phases, respectively, but using different polymer concentrations of (a) 1, (b) 10, (c) 50, and (d) 100 mg/mL. The particles are monodisperse, with a smooth surface and a hole. The holes are visible on only some of the particles, as the particles are randomly arranged on the SEM holders.

suspended in Shandon M-1 embedding matrix (Thermo Scientific, Waltham, MA). Next, a drop of suspension was frozen on aluminum foil in dry ice, and the frozen drop was mounted on a cryostat sample holder. Samples were sectioned with a thickness of 20 μm using a Leica CM 3050 S cryostat (Leica Instruments, Wetzlar, Germany). Both the intact microparticles and the sectioned ones were fastened to a holder using double-sided carbon adhesive tape mounted on an SEM support and platinum coated in a high-vacuum evaporator (Q150TS, Quorum Technologies, East Sussex, U.K.). The images were recorded using a Quanta 250 FEG SEM instrument (FEI Company, Hillsboro, OR). The particle size was measured from the SEM images of prepared microparticles from the same batch. In total, the diameters of more than 150 particles were measured.

2.6. Drug Loading and Release. To determine the amounts of the drugs, SFN and CEL, in the encapsulated microparticles, high-performance liquid chromatography (HPLC, Agilent Technologies, Palo Alto, CA) was used with a Discovery C_{18} column (5 μm, 150 × 4.6 mm, Supelco Analytical, Bellefonte, PA). The two drugs were determined simultaneously with a mobile phase composed of water (1% KH_2PO_4, pH 5.0) and acetonitrile (ratio of 45:55, v/v). The flow rate of the mobile phase was 2 mL/min. The wavelengths used for the detection of CEL and SFN were 254 and 265 nm, respectively.

The produced microparticles with the two drugs encapsulated were separated from the supernatant and washed three times with a Tween 80 solution (2%, w/v). The washed microparticles were dissolved in methanol to release all of the drugs to calculate the drug encapsulation efficiency and the drug loading degree. For drug release, the washed

DOI: 10.1021/acsami.5b04824
ACS Appl. Mater. Interfaces 2015, 7, 14822−14832

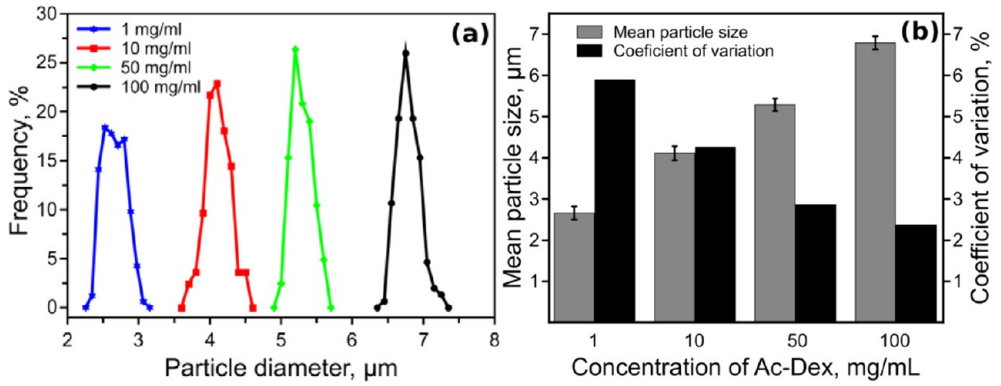

Figure 4. Ac-Dex particle size and uniformity. (a) Microparticle size distribution and (b) mean size with CV as a function of the Ac-Dex polymer concentration. All microparticles were prepared using the same microfluidic device and flow rates of 80 and 20 μL/h for the continuous and dispersed phases, respectively, but with different Ac-Dex concentrations. Error bars represent the mean ± standard deviation (n > 150).

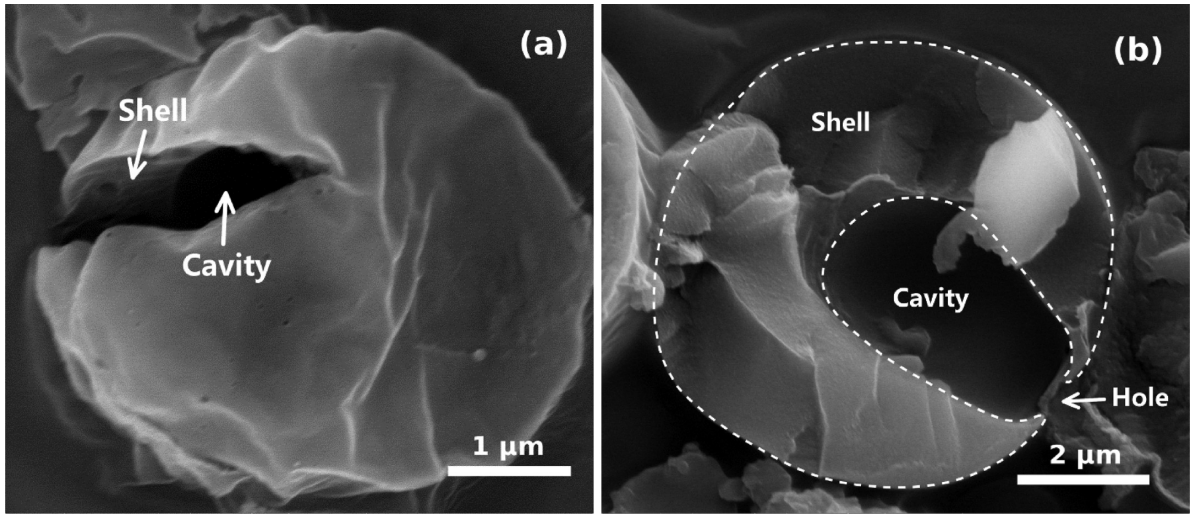

Figure 5. SEM micrographs of Ac-Dex hollow microparticles. (a) Broken particle (3-μm size), revealing the hollow cavity and thickness of the shell. (b) Cryosectioning of a 7-μm particle, with boundaries marked by a dashed line. The microparticles were prepared using the same microfluidic device and flow rates but different polymer concentrations of (a) 10 and (b) 100 mg/mL.

particles were placed in 5 mL of the required pH buffer solution with 2% Tween 80. The drug release studies were conducted at 37 °C with constant stirring at 150 rpm. For the HPLC measurements, samples of 200 μL were taken, centrifuged, and analyzed by HPLC. The volume of removed medium was compensated by adding 200 μL of fresh buffer solution. Samples were taken at 5, 15, 30, 60, and 120 min for each of the pH values tested (2.5, 5.0, and 7.4).

3. RESULTS AND DISCUSSION

3.1. Production of Microparticles. Dripping and jetting are two common regimes employed to generate droplets.[45] For the production of monodisperse droplets and, subsequently, microparticles, the dripping regime is desirable because jetting tends to produce polydisperse droplets and provides limited control over droplet size.[46] In this work, we operated the PDMS microfluidic device in the dripping regime, as determined experimentally using different flow rate parameters (Figure 2). The acetylated dextran (Ac-Dex) solution (10 mg/mL) in dimethyl carbonate (DMC) served as the dispersed phase, and poly(vinyl alcohol) (PVA) solution (2%, w/w) was used as the continuous phase. First, the flow rate of the continuous phase was fixed at 80 μL/h, and the dispersed-phase flow rate was adjusted by varying it from 5 to 60 μL/h (Figure 2a). As shown in Figure 2a, the system became unstable when the solvent flow rate was below 10 μL/h and induced jetting (inset images) at flow rates above 30 μL/h. Subsequently, the flow rate of the dispersed phase was fixed at 15 μL/h, and the flow rate of the continuous phase was adjusted. We noticed that the dripping regime changed to the jetting regime when the continuous-phase flow rate was higher than 120 μL/h or lower than 20 μL/h (Figure 2b and inset images). To maintain a stable dripping regime for long periods of time (>1 h), we chose flow rates far from the threshold values between the two regimes: 20 and 80 μL/h for the dispersed and continuous phases, respectively. Under these flow conditions, the size of the droplets was 20 μm.

Although the initial droplet size was constant and defined by the flow rates of the dispersed and continuous phases, the final microparticle size was significantly affected by the amount of dissolved polymer in the dispersed phase (DMC), as illustrated in the scanning electron microscopy (SEM) images (Figure 3). The size of the particles increased from 2.7 to 6.8 μm when the concentration of the polymer Ac-Dex was increased from 1 to 100 mg/mL (Figure 4). The solidified particles were highly uniform with a coefficient of variation (CV) as low as 2.3% when higher concentrations of polymer were used (Figure 4b). The monodispersity of the microparticles slightly decreased

DOI: 10.1021/acsami.5b04824
ACS Appl. Mater. Interfaces 2015, 7, 14822−14832

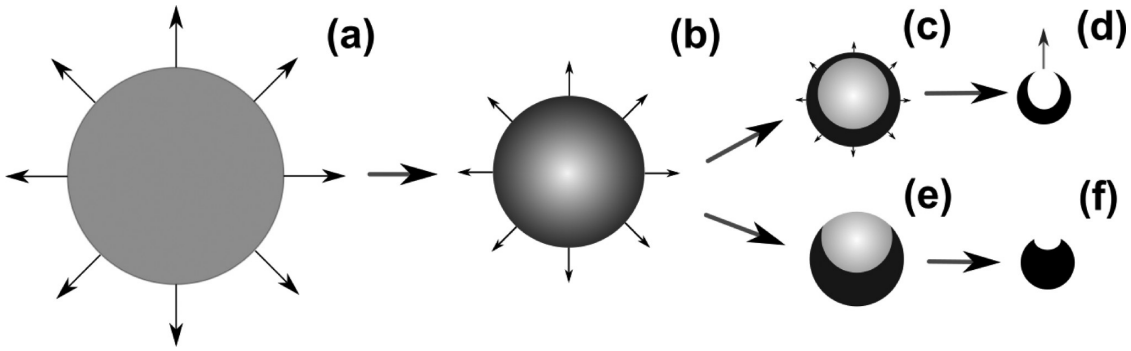

Figure 6. Formation of hollow microparticles induced by solvent diffusion. (a) Solvent diffusion into the continuous phase, (b) polymer accumulation at the solvent−water interface, (c) polymer solidification and phase separation, (d) solvent release and hollow particle formation, (e) solvent droplet and polymer scaffold separation, (f) particle with a dimple.

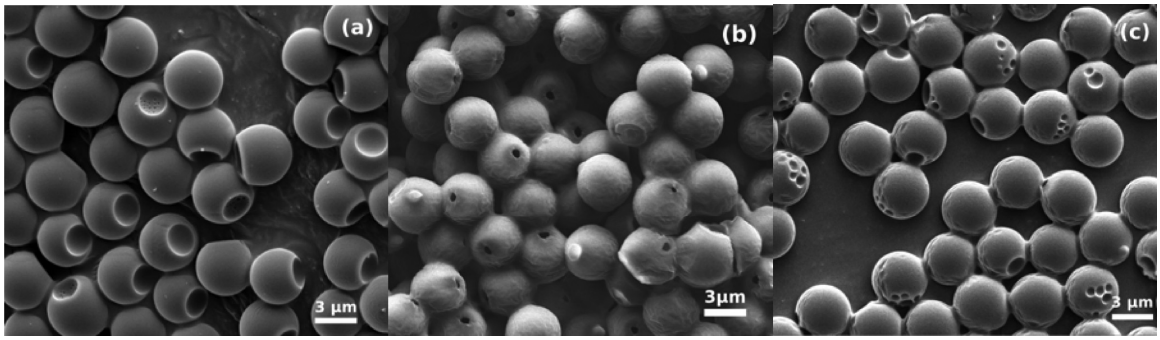

Figure 7. SEM images of microparticles. Microparticles produced using 10 mg/mL concentrations of the polymers (a) Ac-Dex, (b) HPMCAS-HF, and (c) PLGA. The Ac-Dex- and PLGA-based particles contained dimple(s) on the surface, whereas HPMCAS-HF formed hollow particles as witnessed by the appearance of a hole.

(CV ≈ 6%) at lower polymer concentrations, which can be ascribed to the deformation of the microparticles because of their thinner shells.

The increase in the microparticle size was insignificant (~3-fold) compared with the 100-fold increase in the Ac-Dex concentration. This observation can be explained by the hollow structure of the particle (Figures 3 and 5). At low Ac-Dex concentrations, the hollow core occupies most of the volume and has a thin shell, whereas particles produced at high Ac-Dex concentrations have smaller cavities and thicker shells. SEM analysis of the cryosectioned particles prepared with 10 and 100 mg/mL Ac-Dex (Figure 5a,b) confirmed that the particles remained hollow and their shell thickness increased with increasing initial concentration of polymer.

3.2. Hollow Microparticle Formation Mechanism. The formation of hollow microparticles involves different mechanisms and methods. The most common layer-by-layer fabrication technique[17] is based on the deposition of different layers of polymer on a template microparticle, which has to be removed at the end of process by chemical etching. Another common method is based on the encapsulation of gas in the inner phase of double emulsion,[25] where the outer phase consists of a polymer solution that solidifies and forms a solid shell. In this work, the hollow microparticle formation process followed a different mechanism that, based on our results, can be subdivided into the following steps: (a) droplet formation, (b) solvent diffusion into the continuous phase and droplet shrinkage, (c) semisolid or solid shell formation at the water−solvent interface and phase separation, and (d) entrapped solvent release. It is worth noting that, in our system, only droplet generation occurs inside the microfluidic device. Yet, immediately after droplet production, the moderate DMC solubility in water (13.9%) drives solvent diffusion out of the droplet into the continuous phase. Initially, the polymer concentration in the droplet is uniform, and solvent diffusion through the liquid−liquid interface is fast (Figure 6a). The aforementioned solvent diffusion inevitably leads to droplet shrinkage and an increase in polymer viscosity. This process results in a semisolid or solid layer at the droplet interface, where the polymer concentration is the highest (Figure 6b). The solvent diffusion through the dense polymer region starts to decrease exponentially,[18] triggering a further increase in the polymer matrix at the interface[47] and slow phase separation within the inner part of the particle (Figure 6c).[48] The polymer continues to accumulate, making the shell thicker. At this stage, the solvent droplet becomes effectively surrounded by a semisolid polymer shell. During prolonged incubations, the interplay between gravity[19] and interfacial tension forces[49] causes the inner solvent droplet to drift into one side of a particle. This process eventually culminates in the breakup of the outer shell and the release of the inner solvent through the hole (Figure 6d; see also Figures 3 and 5). However, when the polymer concentration is low, phase separation can occur before the polymer forms a solid shell (Figure 6e), which leads to premature solvent release, as witnessed by the appearance of a dimple on the particle surface (Figure 6f). The latter feature was also recorded for particles produced with Ac-Dex (Figure 7a) and PLGA (Figure 7c) polymers.

One could expect that higher concentrations of polymer will lead to thicker shells, making it harder for the trapped solvent to escape and resulting in the formation of a smaller hole (opening). Indeed, we found that encapsulation with higher

DOI: 10.1021/acsami.5b04824
ACS Appl. Mater. Interfaces 2015, 7, 14822−14832

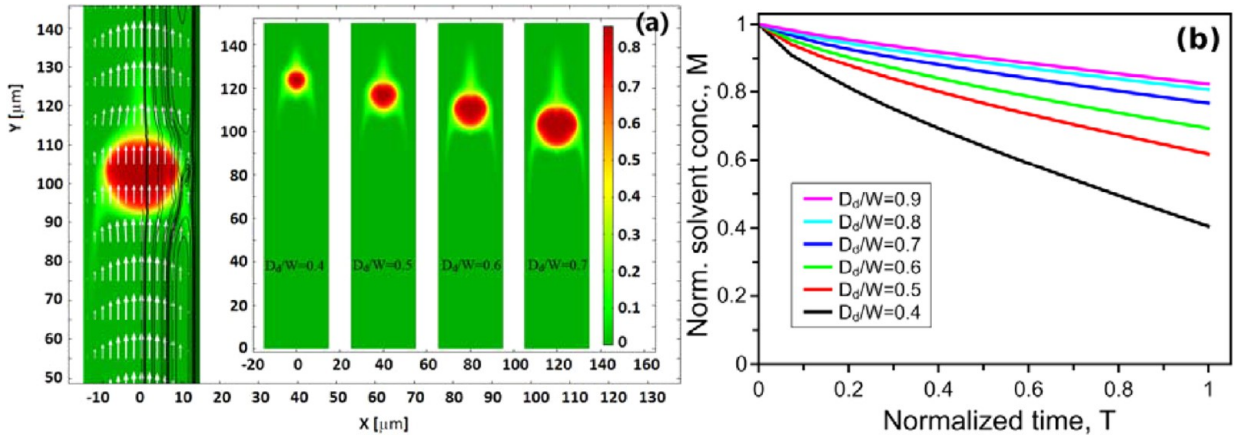

Figure 8. Computer simulation results. (a) Illustration of the mass transfer of the solvent (DMC) out of the droplet as a function of decreasing droplet size D_d (relative to the microchannel width W), as expressed by the ratio D_d/W, from the initial value of 0.9 to a value of 0.4. The vector field, streamlines, and contour of the concentration field illustrate the mass transfer in the vicinity of the droplet. (b) Decay of the normalized solvent (DMC) concentration as a function of D_d/W ratio and time (T) normalized over the length scale of $L = 10D_d/W$. To quantify the effect of the droplet size on mass transfer, the mass of the solvent in the droplet $[m(T) = \int_0^T c\varphi \, dV]$ was calculated at each time step to give the dimensionless mass $\{M(T) = [m(T)]/[m(T = 0)]$, where T is the dimensionless time $[T = (t/L)V_{inlet}]$; V_{inlet} is the velocity at the inlet, which is also the average velocity in the microchannel; and L is the length of the channel}.

concentrations of polymer (100 mg/mL) led to particles with thicker shells (Figure 4) and smaller holes (Figure 3), thereby providing additional support for the model outlined in Figure 6. These results also suggest a simple approach to control of the shell thickness. In principle, the use of even higher polymer concentrations should result in the formation of solid microparticles, similar to that reported recently.[50] However, because of the increased viscosity of the dispersed phase, the dripping regime transitions into jetting, and the resulting droplets become undesirably polydisperse.

The particle formation process is mainly governed by two factors: the diffusion rate of the solvent into the continuous water phase and the convection generated by the inertial forces of the droplet. The combination of these two factors determines the overall mass-transfer rate of the solvent from the inner to the outer phase. Evaluating the contribution of the droplet size to the mass transfer experimentally is challenging because it is difficult to separate the effect of diffusion from the effect of convection during droplet movement. Therefore, we also used a two-phase-flow computational fluid dynamics model to perform a parametric study with varying droplet size D_d, to better understand the roles of diffusion and convection in the kinetics of particle formation.

The presence of the droplet in the middle of the channel alters the Poiseuille flow close to the droplet, inducing two recirculation patterns that can be seen using streamlines (Figure 8a). The velocity field generated by the droplet itself enhances the average mass-transfer rate (of DMC) from the droplet into water due to convection. This effect is proportional to the droplet size (as expressed by the D_d/W ratio). In this work, the initial experimental droplet size was 20 μm, corresponding to an initial D_d/W ratio of about 0.7 (in a microchannel with W = 30 μm). The concentration contours clearly illustrate the gradients of the solvent concentration, quantifying the mass-transfer rate of the solvent through the interface between the two phases (Figure 8a).

Under the experimental conditions used, the mass transfer always remained diffusion-limited, as expressed by the fact that the decay of the normalized DMC concentration was faster for smaller droplets (Figure 8b). However, as a result of convective forces, there is a peak-shape flux toward the front of the droplet in the concentration contours (Figure 8a). This suggests more efficient mass transfer of DMC from inside the droplet toward this direction. On the other hand, the longer it takes for the polymer to precipitate (at low initial polymer concentrations), the smaller the droplet gets (due to solvent diffusion) before precipitation, and the smaller the role of the convective forces on mass transfer from the droplet. This implies that the formation of smaller particles (low initial polymer concentration) is even more diffusion-limited than that of larger particles (high initial polymer concentration), which might be the reason for slightly worse monodispersity (i.e., greater CV) observed for microparticles prepared using low initial polymer concentrations. Therefore, for larger particles, the mass transfer of the solvent from the droplet is more uniform, thus providing higher monodispersity of the microparticles.

It is worth noting that these results are independent of the type of polymer, solvent, and surfactant tested, as long as the solubility differences are similar to those used in the setup presented herein. In this work, the robustness of the microparticle preparation setup was confirmed by the use of three different polymers (HPMCAS-HF, Ac-Dex, and PLGA) (Figure 7). Additionally, two different surfactants (PVA and Pluronic F127) and two solvents (DMC and ethyl acetate) were also tested, but had no influence on the particle shape and size (results not shown). Moreover, the simple design of the microfluidic device provides the possibility for easy scale-up of the system, for example, by applying the design suggested by Nisisako et al.[51]

3.3. Drug Encapsulation and Release. Complex diseases such as lung cancer are often treated with combinations of different drugs.[52] For example, some reports have shown that CEL and SFN can act as an effective drug combination in certain cancer treatments.[53−57] Because of their synergistic effects, smaller drug doses are required, thus minimizing adverse side effects. To test the drug release of CEL and SFN from the particles, we simultaneously encapsulated both drugs in Ac-Dex and HPMCAS-HF microparticles. CEL and SFN are both poorly water-soluble anticancer drugs (maximum solubilities in water of 3.8−15.9 and 4.7−9.3 μg/mL for CEL

DOI: 10.1021/acsami.5b04824
ACS Appl. Mater. Interfaces 2015, 7, 14822−14832

and SFN, respectively). On the other hand, they are highly soluble in DMC (~20 and ~0.5 mg/mL for CEL and SFN, respectively).

The encapsulation efficiency, which is defined as the ratio between the amount of drug encapsulated in the microparticles and the total amount of drugs added to the polymer solution, was high (96–97%) for both CEL and SFN (Table 1). At lower polymer concentrations (10 mg/mL Ac-Dex or HPMCAS-HF), the encapsulation efficiencies decreased to 75–85%, suggesting that, even though lower amounts of drug are encapsulated using lower polymer concentrations, the trapping of the drug molecules within the polymer matrix is still efficient. On the other hand, the loading degree, which is defined as the weight ratio of the loaded drug to the total mass of produced polymer particles with the drugs encapsulated, is inevitably lower for particles prepared with high polymer concentrations and, thus, comprising a greater mass (Table 1). In this work, a loading degree of 0.5% was measured for particles prepared from 100 mg/mL Ac-Dex, but, in theory, higher loading degrees are straightforward to achieve by adding higher concentrations of the drug in the dispersed phase (the only limiting factor being the drug solubility in the solvent).

Table 1. Average Drug Encapsulation for Both Drugs Loaded in the Microparticles

particle	diameter (μm)	encapsulation efficiency (%)	loading degree (%)
100 mg/mL Ac-Dex	6.8 ± 0.1	97 ± 1	0.5 ± 0.2
50 mg/mL Ac-Dex	5.3 ± 0.1	95 ± 1	1.0 ± 0.2
10 mg/mL Ac-Dex	4.1 ± 0.1	85 ± 2	4.2 ± 0.3
10 mg/mL HPMCAS-HF	4.2 ± 0.1	75 ± 4	2.6 ± 0.4

The Ac-Dex and HPMCAS-HF polymers are pH-responsive, and by changing the shell of the hollow microparticles, it is possible to tailor the drug release under different pH conditions. As shown in Figure 9a, the drug release from Ac-Dex hollow microparticles prepared with 100 mg/mL Ac-Dex in DMC solution was less than 10% after 4 h of incubation at pH 7.4 and pH 5.0. As expected, the drug release rate increased when the polymer concentration was decreased. From the microparticles produced with 50 mg/mL Ac-Dex solution, ~20% of the cargo was released (Figure 9b), whereas 30% of the cargo was released from the microparticles prepared with 10 mg/mL Ac-Dex solution after 4 h of incubation (Figure 9c). To accelerate the degradation of Ac-Dex and, thus, the drug release, we reduced the pH value of the buffer to 2.5. Under these conditions, the polymer experienced complete degradation[20] and caused a burst drug release and full release of the encapsulated drugs in less than 5 min. Using HPMCAS-HF hollow microparticles suspended in pH 5.0 buffer, 90% of the drugs was released after 60 min (Figure 9d), whereas at pH 7.4, the drugs had a burst release, and all of the drugs was immediately released in less than 5 min, because of the high dissolution rate of the polymer.

These results show that, regardless of the polymer concentration and the pH value of the release medium used, no significant differences were observed in the release profiles of both CEL and SFN (Figure 9), indicating that the release of the cargo from the hollow microparticles is mainly controlled by the polymer matrix dissolution. The drug release from the Ac-Dex and HPMCAS-HF microparticles can be controlled by different environmental pH values and by changing the polymer concentrations used to produce the microparticles. Thus, we anticipate that, by using a microfluidics approach similar to that presented here, it will be possible to fabricate

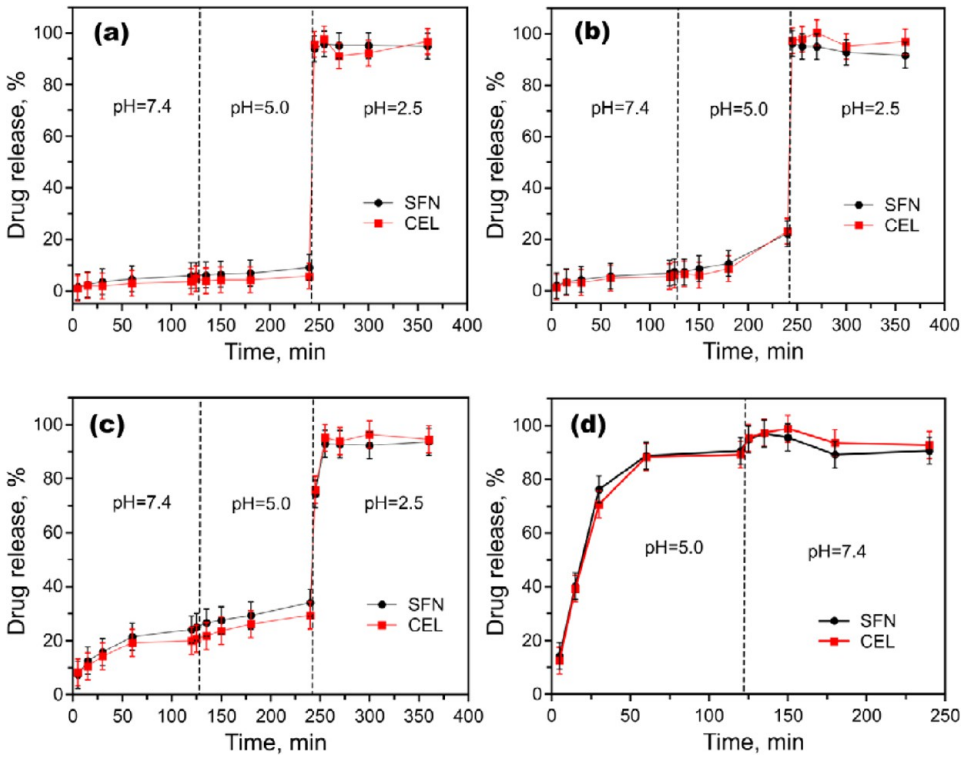

Figure 9. Release profiles of CEL and SFN from microparticles prepared with different polymer concentrations: (a) 100 mg/mL Ac-Dex, (b) 50 mg/mL Ac-Dex, (c) 10 mg/mL Ac-Dex, and (d) 10 mg/mL HPMCAS-HF. Error bars represent the mean ± standard deviation (n = 3).

DOI: 10.1021/acsami.5b04824
ACS Appl. Mater. Interfaces 2015, 7, 14822–14832

hollow microparticles for drug-delivery and biomedical applications.

4. CONCLUSIONS

We have demonstrated a simple and robust way to produce monodisperse hollow microparticles with controlled size using a flow-focusing PDMS-based microfluidic device. The formation of particles smaller than 10 μm was initiated by solvent diffusion followed by shell formation upon polymer solidification. Numerical calculations showed that, despite the presence of convective recirculation around the droplet, the mass-transfer rate of the solvent dissolution from the droplet to the surrounding phase was still dominated by diffusion. Control of the particle size and the rate of drug release was demonstrated by the production of particles with different types of polymers and polymer concentrations. The encapsulation efficiency in Ac-Dex polymer microparticles was high (96−97%) for both model anticancer drugs, CEL and SFN, when a high polymer concentration was used (100 mg/mL), whereas at a lower polymer concentration (10 mg/mL Ac-Dex or HPMCAS-HF), the encapsulation efficiency decreased to 75−85%. Both drugs were released simultaneously as a result of polymer matrix dissolution, making the particles suitable for multidrug delivery. Moreover, by controlling the shell thickness and the size of the hollow core, it should be possible to adjust the mass density of the particles and provide an additional level of control for improved pulmonary drug delivery. Finally, the nontoxic materials, small size (<7 μm), and hollow structure of the microparticles provide a highly promising approach for preparing pulmonary drug-delivery systems and controlled drug release.

AUTHOR INFORMATION

Corresponding Authors

*Tel.: +370-693-19333. Fax +370 52602116. E-mail: linas.mazutis@bti.vu.lt.

*Tel.: +358 2941 59661. E-mail: helder.santos@helsinki.fi.

Notes

The authors declare no competing financial interest.

ACKNOWLEDGMENTS

R.V. acknowledges postdoctoral fellowship from the European Union Structural Funds Project "Postdoctoral Fellowship Implementation in Lithuania" (VP1-3.1-SMM-01). H.A.S. acknowledges financial support from the Academy of Finland (Grants 252215 and 281300), the University of Helsinki Research Funds, the Biocentrum Helsinki, and the European Research Council (FP/2007−2013, Grant 310892). H.Z. acknowledges the Jane and Aatos Erkko Foundation for financial support (Grant 4704010). T.S. acknowledges the University of Helsinki Research Funds, the Academy of Finland (Grant 251629), and the European Research Council (Grant 311705). L.M. acknowledges financial support from the Lithuanian Agency for Science, Innovation and Technology (MITA, uVesicles 31v-40). The authors are thankful to Reeta Huhtala from the Tissue and Histochemistry Unit, Faculty of Medicine, University of Helsinki, for the cryosection of the microparticles. We thank the Electron Microscopy Unit of the Institute of Biotechnology, University of Helsinki, for providing laboratory facilities for SEM imaging.

REFERENCES

(1) Anselmo, A. C.; Mitragotri, S. An Overview of Clinical and Commercial Impact of Drug Delivery Systems. *J. Controlled Release* **2014**, *190*, 15−28.

(2) Jain, K. K. Drug Delivery Systems—An Overview. *Methods Mol. Biol.* **2008**, *437*, 1−50.

(3) Coelho, J. F.; Ferreira, P. C.; Alves, P.; Cordeiro, R.; Fonseca, A. C.; Góis, J. R.; Gil, M. H. Drug Delivery Systems: Advanced Technologies Potentially Applicable in Personalized Treatments. *EPMA J.* **2010**, *1* (1), 164−209.

(4) Lee, W.; Park, J.; Yang, E. H.; Suh, H.; Kim, S. H.; Chung, D. S.; Choi, K.; Yang, C. W.; Park, J. Investigation of the Factors Influencing the Release Rates of Cyclosporin A-Loaded Micro- and Nanoparticles Prepared by High-Pressure Homogenizer. *J. Controlled Release* **2002**, *84*, 115−123.

(5) Campos, E.; Branquinho, J.; Carreira, A. S.; Carvalho, A.; Coimbra, P.; Ferreira, P.; Gil, M. H. Designing Polymeric Microparticles for Biomedical and Industrial Applications. *Eur. Polym. J.* **2013**, *49* (8), 2005−2021.

(6) Xu, Q.; Hashimoto, M.; Dang, T. T.; Hoare, T.; Kohane, D. S.; Whitesides, G. M.; Langer, R.; Anderson, D. G. Preparation of Monodisperse Biodegradable Polymer Microparticles Using a Microfluidic Flow-Focusing Device for Controlled Drug Delivery. *Small* **2009**, *5* (13), 1575−1581.

(7) Kong, T.; Wu, J.; To, M.; Wai Kwok Yeung, K.; Cheung Shum, H.; Wang, L. Droplet Based Microfluidic Fabrication of Designer Microparticles for Encapsulation Applications. *Biomicrofluidics* **2012**, *6* (3), 34104.

(8) Wan, F.; Bohr, A.; Maltesen, M. J.; Bjerregaard, S.; Foged, C.; Rantanen, J.; Yang, M. Critical Solvent Properties Affecting the Particle Formation Process and Characteristics of Celecoxib-Loaded PLGA Microparticles via Spray-Drying. *Pharm. Res.* **2013**, *30* (4), 1065−1076.

(9) Seemann, R.; Brinkmann, M.; Pfohl, T.; Herminghaus, S. Droplet Based Microfluidics. *Rep. Prog. Phys.* **2012**, *75* (1), 016601.

(10) Scheuch, G.; Kohlhaeufl, M. J.; Brand, P.; Siekmeier, R. Clinical Perspectives on Pulmonary Systemic and Macromolecular Delivery. *Adv. Drug Delivery Rev.* **2006**, *58* (9−10), 996−1008.

(11) Liang, Z.; Ni, R.; Zhou, J.; Mao, S. Recent Advances in Controlled Pulmonary Drug Delivery. *Drug Discovery Today* **2014**, *20* (3), 380−389.

(12) Meenach, S. A.; Kim, Y. J.; Kauffman, K. J.; Kanthamneni, N.; Bachelder, E. M.; Ainslie, K. M. Synthesis, Optimization, and Characterization of Camptothecin-Loaded Acetalated Dextran Porous Microparticles for Pulmonary Delivery. *Mol. Pharm.* **2012**, *9* (2), 290−298.

(13) Liu, D.; Herranz-Blanco, B.; Mäkilä, E.; Arriaga, L. R.; Mirza, S.; Weitz, D. A.; Sandler, N.; Salonen, J.; Hirvonen, J.; Santos, H. A. Microfluidic Templated Mesoporous Silicon−Solid Lipid Microcomposites for Sustained Drug Delivery. *ACS Appl. Mater. Interfaces* **2013**, *5* (22), 12127−12134.

(14) Zhang, H.; Liu, D.; Shahbazi, M.-A.; Mäkilä, E.; Herranz-Blanco, B.; Salonen, J.; Hirvonen, J.; Santos, H. A. Fabrication of a Multifunctional Nano-in-Micro Drug Delivery Platform by Microfluidic Templated Encapsulation of Porous Silicon in Polymer Matrix. *Adv. Mater.* **2014**, *26* (26), 4497−4503.

(15) Liu, D.; Zhang, H.; Herranz-Blanco, B.; Mäkilä, E.; Lehto, V.-P.; Salonen, J.; Hirvonen, J.; Santos, H. A. Microfluidic Assembly of Monodisperse Multistage pH-Responsive Polymer/Porous Silicon Composites for Precisely Controlled Multi-Drug Delivery. *Small* **2014**, *10* (10), 2029−2038.

(16) Edwards, D. A.; Hanes, J.; Caponetti, G.; Hrkach, J.; Ben-Jebria, A.; Eskew, M.; Lou; Mintzes, J.; Deaver, D.; Lotan, N.; Langer, R. Large Porous Particles for Pulmonary Drug Delivery. *Science* **1997**, *276* (5320), 1868−1871.

(17) Feng, D.; Shi, J.; Wang, X.; Zhang, L.; Cao, S. Hollow Hybrid Hydroxyapatite Microparticles with Sustained and pH-Responsive Drug Delivery Properties. *RSC Adv.* **2013**, *3* (47), 24975.

DOI: 10.1021/acsami.5b04824
ACS Appl. Mater. Interfaces 2015, 7, 14822−14832

(18) Li, W.; Anderson, K. W.; Mehta, R. C.; Deluca, P. P. Prediction of Solvent Removal Profile and Effect on Properties for Peptide-Loaded PLGA Microspheres Prepared by Solvent Extraction/Evaporation Method. *J. Controlled Release* **1995**, *37* (3), 199−214.
(19) Datta, S. S.; Abbaspourrad, A.; Amstad, E.; Fan, J.; Kim, S.-H.; Romanowsky, M.; Shum, H. C.; Sun, B.; Utada, A. S.; Windbergs, M.; Zhou, S.; Weitz, D. A. 25th Anniversary Article: Double Emulsion Templated Solid Microcapsules: Mechanics and Controlled Release. *Adv. Mater.* **2014**, *26* (14), 2205−2218.
(20) Liu, D.; Zhang, H.; Mäkilä, E.; Fan, J.; Herranz-Blanco, B.; Wang, C.-F.; Rosa, R.; Ribeiro, A. J.; Salonen, J.; Hirvonen, J.; Santos, H. A. Microfluidic Assisted One-Step Fabrication of Porous Silicon@acetalated Dextran Nanocomposites for Precisely Controlled Combination Chemotherapy. *Biomaterials* **2015**, *39*, 249−259.
(21) Chang, J.-Y.; Yang, C.-H.; Huang, K.-S. Microfluidic Assisted Preparation of CdSe/ZnS Nanocrystals Encapsulated into Poly(DL-lactide-*co*-glycolide) Microcapsules. *Nanotechnology* **2007**, *18*, 305305.
(22) Lin, Y. S.; Yang, C.-H.; Wang, C. Y.; Chang, F. R.; Huang, K. S.; Hsieh, W. C. An Aluminum Microfluidic Chip Fabrication Using a Convenient Micromilling Process for Fluorescent Poly(DL-lactide-*co*-glycolide) Microparticle Generation. *Sensors* **2012**, *12* (2), 1455−1467.
(23) Yang, C.-H.; Huang, K. S.; Grumezescu, A. M.; Wang, C. Y.; Tzeng, S. C.; Chen, S. Y.; Lin, Y. H.; Lin, Y. S. Synthesis of Uniform Poly(D,L-lactide) and Poly(D,L-lactide-*co*-glycolide) Microspheres Using a Microfluidic Chip for Comparison. *Electrophoresis* **2014**, *35* (2−3), 316−322.
(24) Karnik, R.; Gu, F.; Basto, P.; Cannizzaro, C.; Dean, L.; Kyei-Manu, W.; Langer, R.; Farokhzad, O. C. Microfluidic Platform for Controlled Synthesis of Polymeric Nanoparticles. *Nano Lett.* **2008**, *8* (9), 2906−2912.
(25) Chen, R.; Dong, P.-F.; Xu, J.-H.; Wang, Y.-D.; Luo, G.-S. Controllable Microfluidic Production of Gas-in-Oil-in-Water Emulsions for Hollow Microspheres with Thin Polymer Shells. *Lab Chip* **2012**, *12* (20), 3858−3860.
(26) Watanabe, T.; G Lopez, C.; Douglas, J. F.; Ono, T.; Cabral, J. T. Microfluidic Approach to the Formation of Internally Porous Polymer Particles by Solvent Extraction. *Langmuir* **2014**, *30* (9), 2470−2479.
(27) Nie, Z.; Xu, S.; Seo, M.; Lewis, P. C.; Kumacheva, E. Polymer Particles with Various Shapes and Morphologies Produced in Continuous Microfluidic Reactors. *J. Am. Chem. Soc.* **2005**, *127* (22), 8058−8063.
(28) Edwards, D.; Dunbar, C. Bioengineering of Therapeutic Aerosols. *Annu. Rev. Biomed. Eng.* **2002**, *4*, 93−107.
(29) Chono, S.; Tanino, T.; Seki, T.; Morimoto, K. Influence of Particle Size on Drug Delivery to Rat Alveolar Macrophages Following Pulmonary Administration of Ciprofloxacin Incorporated into Liposomes. *J. Drug Target* **2006**, *14* (8), 557−566.
(30) Labiris, N. R.; Dolovich, M. B. Pulmonary Drug Delivery. Part I: Physiological Factors Affecting Therapeutic Effectiveness of Aerosolized Medications. *Br. J. Clin. Pharmacol.* **2003**, *56* (6), 588−599.
(31) Dendukuri, D.; Doyle, P. S. The Synthesis and Assembly of Polymeric Microparticles Using Microfluidics. *Adv. Mater.* **2009**, *21* (41), 4071−4086.
(32) Hung, L.-H.; Teh, S.-Y.; Jester, J.; Lee, A. P. PLGA Micro/Nanosphere Synthesis by Droplet Microfluidic Solvent Evaporation and Extraction Approaches. *Lab Chip* **2010**, *10* (14), 1820−1825.
(33) Wan, J. Microfluidic-Based Synthesis of Hydrogel Particles for Cell Microencapsulation and Cell-Based Drug Delivery. *Polymers (Basel, Switz.)* **2012**, *4* (4), 1084−1108.
(34) Martinez, C. J.; Kim, J. W.; Ye, C.; Ortiz, I.; Rowat, A. C.; Marquez, M.; Weitz, D. A Microfluidic Approach to Encapsulate Living Cells in Uniform Alginate Hydrogel Microparticles. *Macromol. Biosci.* **2012**, *12* (7), 946−951.
(35) Liu, K.; Deng, Y.; Zhang, N.; Li, S.; Ding, H.; Guo, F.; Liu, W.; Guo, S.; Zhao, X.-Z. Generation of Disk-like Hydrogel Beads for Cell Encapsulation and Manipulation Using a Droplet-Based Microfluidic Device. *Microfluid. Nanofluid.* **2012**, *13* (5), 761−767.
(36) Cito, S.; Ahn, Y.-C.; Pallares, J.; Duarte, R. M.; Chen, Z.; Madou, M.; Katakis, I. Visualization and Measurement of Capillary-Driven Blood Flow Using Spectral Domain Optical Coherence Tomography. *Microfluid. Nanofluid.* **2012**, *13* (2), 227−237.
(37) Cito, S.; Pallares, J.; Fabregat, A.; Katakis, I. Numerical Simulation of Wall Mass Transfer Rates in Capillary-Driven Flow in Microchannels. *Int. Commun. Heat Mass Transfer* **2012**, *39* (8), 1066−1072.
(38) Ahn, Y.-C.; Jung, W.; Chen, Z. Optical Sectioning for Microfluidics: Secondary Flow and Mixing in a Meandering Microchannel. *Lab Chip* **2008**, *8* (1), 125−133.
(39) Mazutis, L.; Gilbert, J.; Ung, W. L.; Weitz, D. A.; Griffiths, A. D.; Heyman, J. A. Single-Cell Analysis and Sorting Using Droplet-Based Microfluidics. *Nat. Protoc.* **2013**, *8* (5), 870−891.
(40) Bauer, W.-A. C.; Fischlechner, M.; Abell, C.; Huck, W. T. S. Hydrophilic PDMS Microchannels for High-Throughput Formation of Oil-in-Water Microdroplets and Water-in-Oil-in-Water Double Emulsions. *Lab Chip* **2010**, *10* (14), 1814−1819.
(41) Tundo, P.; Selva, M. The Chemistry of Dimethyl Carbonate. *Acc. Chem. Res.* **2002**, *35* (9), 706−716.
(42) Devrim, B.; Bozkir, A.; Canefe, K. Preparation and Evaluation of PLGA Microparticles as Carrier for the Pulmonary Delivery of rhIL-2: I. Effects of Some Formulation Parameters on Microparticle Characteristics. *J. Microencapsulation* **2011**, *28* (6), 582−594.
(43) Thomasin, C.; Merkle, H. P.; Gander, B. Drug Microencapsulation by PLA/PLGA Coacervation in the Light of Thermodynamics. 2. Parameters Determining Microsphere Formation. *J. Pharm. Sci.* **1998**, *87* (3), 269−275.
(44) Yue, P.; Zhou, C.; Feng, J. J. Spontaneous Shrinkage of Drops and Mass Conservation in Phase-Field Simulations. *J. Comput. Phys.* **2007**, *223* (1), 1−9.
(45) Clanet, C.; Lasheras, J. C. Transition from Dripping to Jetting. *J. Fluid Mech.* **1999**, *383*, 307−326.
(46) Ambravaneswaran, B.; Subramani, H.; Phillips, S.; Basaran, O. Dripping-Jetting Transitions in a Dripping Faucet. *Phys. Rev. Lett.* **2004**, *93* (3), 034501.
(47) Shim, J.; Cristobal, G.; Link, D. R.; Thorsen, T.; Jia, Y.; Piattelli, K.; Fraden, S. Control and Measurement of the Phase Behavior of Aqueous Solutions Using Microfluidics. *J. Am. Chem. Soc.* **2007**, *129* (28), 8825−8835.
(48) De Gennes, P.-G. Solvent Evaporation of Spin Cast Films: Crust Effects. *Eur. Phys.* **2002**, *7*, 31−34.
(49) Zarzar, L. D.; Sresht, V.; Sletten, E. M.; Kalow, J. A.; Blankschtein, D.; Swager, T. M. Dynamically Reconfigurable Complex Emulsions via Tunable Interfacial Tensions. *Nature* **2015**, *518* (7540), 520−524.
(50) Ono, T.; Yamada, M.; Suzuki, Y.; Taniguchi, T.; Seki, M. One-Step Synthesis of Spherical/Nonspherical Polymeric Microparticles Using Non-Equilibrium Microfluidic Droplets. *RSC Adv.* **2014**, *4* (26), 13557.
(51) Nisisako, T.; Torii, T.; Takahashi, T.; Takizawa, Y. Synthesis of Monodisperse Bicolored Janus Particles with Electrical Anisotropy Using a Microfluidic Co-Flow System. *Adv. Mater.* **2006**, *18* (9), 1152−1156.
(52) Gravitz, L. Chemoprevention: First Line of Defence. *Nature* **2011**, *471* (7339), S5−S7.
(53) Rosendahl, A. H.; Gundewar, C.; Said, K.; Karnevi, E.; Andersson, R. Celecoxib Synergizes Human Pancreatic Ductal Adenocarcinoma Cells to Sorafenib-Induced Growth Inhibition. *Pancreatology* **2012**, *12* (3), 219−226.
(54) Morisaki, T.; Umebayashi, M.; Kiyota, A.; Koya, N.; Tanaka, H.; Onishi, H.; Katano, M. Combining Celecoxib with Sorafenib Synergistically Inhibits Hepatocellular Carcinoma Cells in Vitro. *Anticancer Res.* **2013**, *33*, 1387−1395.
(55) Liu, Y.; Liu, A.; Li, H.; Li, C.; Lin, J. Celecoxib Inhibits Interleukin-6/Interleukin-6 Receptor-Induced JAK2/STAT3 Phosphorylation in Human Hepatocellular Carcinoma Cells. *Cancer Prev. Res.* **2011**, *4* (8), 1296−1305.
(56) Cervello, M.; Bachvarov, D.; Lampiasi, N.; Cusimano, A.; Azzolina, A.; McCubrey, J. A.; Montalto, G. Novel Combination of Sorafenib and Celecoxib Provides Synergistic Anti-Proliferative and

DOI: 10.1021/acsami.5b04824
ACS Appl. Mater. Interfaces 2015, 7, 14822−14832

Pro-Apoptotic Effects in Human Liver Cancer Cells. *PLoS One* **2013**, *8* (6), e65569.
(57) Escudier, B.; Eisen, T.; Stadler, W. M.; Szczylik, C.; Siebels, M.; Negrier, S.; Chevreau, C.; Solska, E.; Desai, A. A.; Demkow, T.; Hutson, T. E.; Gore, M.; Freeman, S.; Schwartz, B.; Shan, M.; Simantov, R.; Bukowski, R. M. Sorafenib in Advanced Clear-Cell Renal-Cell Carcinoma. *N. Engl. J. Med.* **2007**, *356*, 125−134.

DOI: 10.1021/acsami.5b04824
ACS Appl. Mater. Interfaces 2015, 7, 14822−14832